SINGLE VOLUME PROCEEDINGS

CICE 2023

RIO DE JANEIRO - BRAZIL

11TH INTERNATIONAL CONFERENCE ON FRP COMPOSITES IN CIVIL ENGINEERING

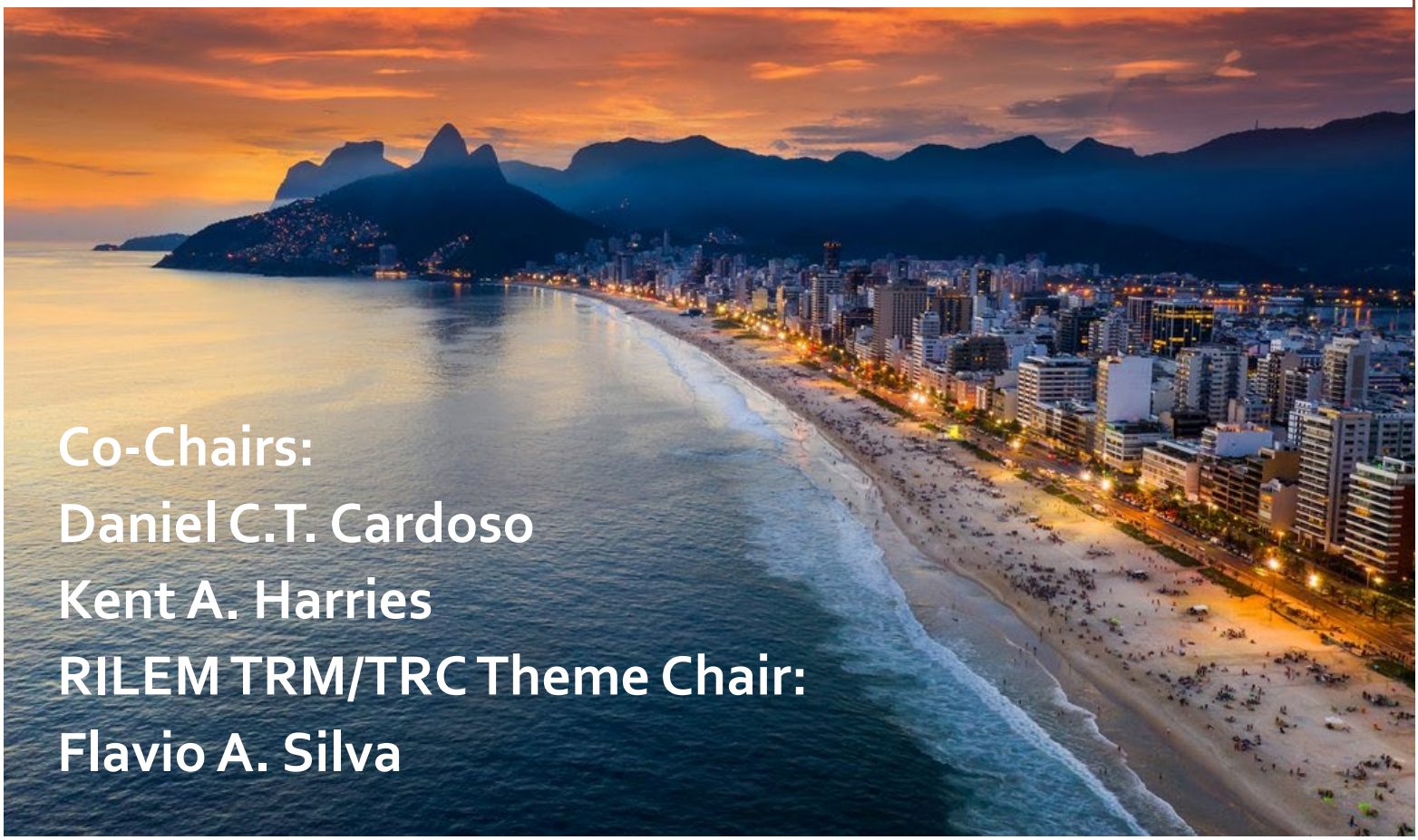

Co-Chairs:

Daniel C.T. Cardoso

Kent A. Harries

RILEM TRM/TRC Theme Chair:

Flavio A. Silva

This proceedings is a single volume version of the the dynamic Proceedings available on Zenodo:

https://zenodo.org/communities/cice2023/

Each paper is also available individually on Zenodo and is assigned a unique DOI: 10.5281/zenodo.8205789

Meeting:

11th International Conference on Fiber-Reinforced Polymer (FRP) Composites in Civil Engineering (CICE 2023), Rio de Janeiro, Brazil, 24-26 July 2023

When citing papers from this conference, please include Paper Number. 251

Welcome to Rio!

Welcome to the 11th International Conference on Fiber-Reinforced Polymer (FRP) Composites in Civil Engineering (CICE 2023)!

Welcome to the International FRP community's first face to face conference in five years!

CICE 2023 is the eleventh in a series of prestigious conferences that began in 2001, in Hong Kong, and has circled the world since; this is the first CICE to be held in South America.

CICE is the official conference of International Institute for FRP in Construction (IIFC) and brings together the FRP research community and industry to share and discuss recent developments and future perspectives in the field.

FULL CONFERENCE PROCEEDINGS
zenodo.org/communities/cice2023/

CICE 2023 WEBSITE
cice2023.org

CICE 2023 BY THE NUMBERS

332 abstracts received... 196 papers published... representing 519 authors... and 36 countries

PAST CICE CONFERENCES

2001 Hong Kong
2004 Adelaide, Australia
2006 Miami, USA
2008 Zurich, Switzerland
2010 Beijing, China
2012 Rome, Italy
2014 Vancouver, Canada
2016 Hong Kong
2018 Paris, France
2021 Istanbul, Turkiye

CICE 2023
Rio de Janeiro - Brazil
11TH INTERNATIONAL CONFERENCE ON FRP COMPOSITES IN CIVIL ENGINEERING

Conference Co-Chairs

Daniel C. T. Cardoso – Pontifical Catholic University of Rio de Janeiro, Brazil
Kent A. Harries – University of Pittsburgh, USA

Organizing Committee

Flávio A. Silva – Pontifical Catholic University of Rio de Janeiro, Brazil
Janine Vieira – Fluminense Federal University, Brazil
Martin Noël – University of Ottawa, Canada
TianQiao Liu – Beijing University of Technology, China
Rebecca Gravina – The University of Queensland, Australia

Local Organization

Ana Luiza de Moura Rodrigues
Bluma Gamerman
Bruno Jordão
Euclides Moura Neto
Felipe Souza Rodrigues
Geovane Silva
Gilcyvania Costa
Gisele Cintra
Iranildo Silva Junior
Jessé Beserra
Jon Karl Weibull
Julio Jorge Braga de Carvalho Nunes
Kíssila Goliath
Lilia Cruz
Luisa Frade
Marcello Tostes
Natália Victoria dos Santos
Paulo Henrique Marangoni Feghali
Priscilla Shimba Carneiro Vieira
Rebecca Mansur de Castro Silva
Renan Felinto dos Santos
Rennan Liberato Rodrigues
Rita de Cassia N. Leite
Thiago Andrade Gomes
Vitor Monteiro
Victor Nascimento Silva

Alessandra Leitão (Creacteve Eventos)
Marcus Moura (VOAR Multimedia)

CICE2023 Rio de Janeiro – Brazil 11TH INTERNATIONAL CONFERENCE ON FRP COMPOSITES IN CIVIL ENGINEERING

BEHAVIOR OF CONCRETE BEAMS REINFORCED WITH STEEL BARS OR THERMOSET AND THERMOPLASTIC RESIN GFRP BARS

Tommaso D'Antino, Politecnico di Milano, Italy, tommaso.dantino@polimi.it
Bertolli Veronica, Politecnico di Milano, Italy, veronica.bertolli@polimi.it
Marco Andrea Pisani, Politecnico di Milano, Italy, marcoandrea.pisani@polimi.it
Carlo Poggi, Politecnico di Milano, Italy, carlo.poggi@polimi.it

ABSTRACT
Fiber-reinforced polymer (FRP) bars have peculiar mechanical and physical properties that make them a viable alternative to traditional steel bars to reinforce concrete members, particularly in the case of aggressive environments. GFRP bars can be made with thermosetting or thermoplastic resins. While in the former case research has been done for several years, limited knowledge is available regarding the behavior of concrete members reinforced with thermoplastic bars. In this paper, the experimental behavior of concrete beams reinforced with steel and thermoset or thermoplastic GFRP bars is compared, showing the effectiveness of both types of bar when adopted as internal reinforcement.

KEYWORDS
GFRP bars; thermoplastic resin; beam; bending; shear.

INTRODUCTION
Fiber-reinforced polymer (FRP) bars represent an effective alternative to traditional steel bars for reinforcing concrete members in specific service conditions. In particular, FRP bars provide important advantages over steel bars in aggressive environments, such as in coastal regions where the presence of salts promotes the steel bar corrosion. Due to the absence of corrosion, FRP bars also potentially allow for reducing the concrete cover thickness (Federation Internationale du Beton, 2007).

FRP bars comprise high-strength fibers and an organic matrix. Carbon, glass, basalt, and aramid fibers are usually employed, whereas thermoset vinylester and polyester resins are generally employed as matrix. Among possible types of FRP bar, glass FRP (GFRP) bars are the most diffused due to their high mechanical properties and low cost with respect to other bar types. GFRP bars have a linear elastic behavior both in tension and compression (D'Antino & Pisani, 2023). They have high tensile strength (usually between 800 MPa and 1200 MPa (D'Antino et al., 2018)) and an elastic modulus usually between 20 and 25% of that of steel. Although GFRP bars have been employed to reinforce concrete members for more than two decades (Ahmed et al., 2014), some issues still need investigation, such as the bar-concrete stress transfer mechanism and fatigue behavior of GFRP-reinforced concrete members (Carvelli et al., 2010; Januš et al., 2019; Solyom & Balázs, 2020; Zhao et al., 2022). Recently, thermoplastic matrices have been proposed to realize FRP bars (Benmokrane et al., 2021; D'Antino et al., 2023). With this type of resin, the bar can be shaped multiple times just heating the resin, which in turn allows for coiling and transporting the bar that will be cut and shaped on site thus saving cost, time, and material. Furthermore, thermoplastic bars provide better recyclability than thermosetting bars (Zoller et al., 2019).

The state of research on thermoplastic bars is still quite limited. Limited work was done mainly to assess the mechanical and physical properties of thermoplastic bars (Benmokrane et al., 2021; D'Antino & Pisani, 2023; Kocaoz et al., 2005), whereas research is still needed to investigate the behavior of concrete members reinforced with this type of bars.

In this paper, the results of bending tests of concrete beams reinforced with traditional steel bars and with thermosetting or thermoplastic resin GFRP bars are presented and discussed. Four beams are

tested, each reinforced with both longitudinal and transversal (i.e., stirrups) bars of the same type. The same cross-sectional area of longitudinal reinforcing bars is considered in all beams. In addition to the beam reinforced with steel bars, one beam is reinforced with straight longitudinal thermoset GFRP bars, one with straight longitudinal thermoplastic GFRP bars, and one with longitudinal thermoplastic GFRP bars that were bent at the end to investigate the effectiveness of this shape in improving the bar anchorage. The same shear reinforcement ratio is considered for each beam and bar type. The results obtained are compared in terms of beam load response, mode of failure, and cracking and peak loads. Furthermore, shear and bending capacities of the tested beams were computed according to the Eurocode 2 (European Committee for Standardization, 2004), *fib* Bulletin 40 (Federation Internationale du Beton, 2007), and CNR-DT 203 (National Research Council, 2007), allowing for assessing the accuracy of the formulations proposed by these documents. These results show that thermoset and thermoplastic GFRP bars provide similar behavior and can be effectively employed as an alternative to steel bars.

MATERIALS AND METHODS

The four beams were cast from the same concrete batch. The concrete compressive strength was measured by testing three 150×150×150 mm cubes cast from the same concrete batch used for the beams (European Committee for Standardization, 2019). The average compressive strength obtained at 28 days was R_{cm}=54.0 MPa (CoV=3.65%), which provided an average cylindrical compressive strength f_{cm}=0.83R_{cm}=44.8 MPa (European Committee for Standardization, 2004).

The longitudinal reinforcement was comprised of bars with nominal diameter ϕ_{no}=12 mm, whereas stirrups were made with bars with nominal diameter ϕ_{no}=6 mm. Ribbed steel bars type B450C were employed for the longitudinal and transversal reinforcement. Tensile testing of three steel bar specimens with ϕ_{no}=12 mm (Figure 1) provided the average elastic modulus E_s=195.82 GPa, average yield strength f_{ym}=505 MPa and average peak strength f_{um}=631 MPa.
Thermoset GFRP bars had a sand-coated surface with a carbon yarn externally wrapped at a spacing of approximately 24 mm (Figure 1). Thermoplastic GFRP bars had a grooved surface with grooves spaced at approximately 40 mm (Figure 1). The average tensile strength $\overline{\sigma}_f^*$ and average elastic modulus $\overline{E}_f$ of the bars were obtained by tensile tests according to (ISO 10406-1:2015, 2015). The results obtained are reported in Table 1, where # is the number of specimens tested, ϕ_{ef} is the effective diameter computed by the immersion method (ISO 10406-1:2015, 2015) and considered to obtain $\overline{\sigma}_f^*$ and $\overline{E}_f$, and values between parentheses are the coefficients of variation (in %). Further details regarding these tests can be found in (D'Antino et al., 2023; D'Antino & Pisani, 2023).

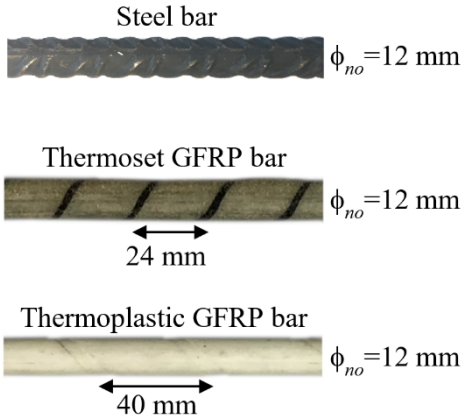

Figure 1: Steel, thermoset GFRP, and thermoplastic GFRP bars

Table 1: Mechanical properties of reinforcing bars (D'Antino et al., 2023; D'Antino & Pisani, 2023)

Bar type	#	ϕ_{no} [mm]	ϕ_{ef} [mm]	E_s [GPa]	f_{ym} [MPa]	f_{um} [MPa]	$\bar{E}_f$ [GPa]	$\bar{\sigma}^*_f$ [MPa]
Steel	5	12	12.0	195.82(3.51)	505 (3.00)	631 (0.98)		
GFRP thermoset	5	6	6.1				54.46 (0.21)	1220 (3.77)
	10	12	12.7				47.73 (1.94)	1040 (3.46)
GFRP thermoplastic	10	6	6.1				53.57 (1.00)	1030 (3.84)
	10	12	12.9				52.69 (1.10)	1030 (3.20)

Beam reinforcement and test set-up

The beams had a rectangular cross-section with height h=300 mm and width b_w=250 mm. Each beam was reinforced with 5 longitudinal bars in tension with nominal diameter ϕ_{no}=12 mm, 2 longitudinal bars in compression with the same diameter, and stirrups with nominal diameter ϕ_{no}=6 mm spaced at 100 mm on center. The overall length of the beam was 3000 mm (Figure 2). The ends of the steel longitudinal bars in tension were bent to provide sufficient anchorage length. To investigate the effectiveness of the bar bending in the case of GFRP bars, in one beam the longitudinal GFRP thermoplastic bars in tension were bent at the end, whereas in another beam they were straight. The longitudinal GFRP thermoset bars in tension were straight (Figure 2).

A four-point bending test set-up was adopted, with a distance between the support axes equal to 2400 mm and a distance between the load application points equal to 600 mm. The beams were supported by a hinge on one side and a roller on the opposite side, while the two loads were applied using a spreader beam connected to a 1000 kN capacity hydraulic jack. Two hinge supports were placed between the spreader beam and the specimen. The applied load P was measured by a load cell placed between the hydraulic jack and the spreader beam. The beam vertical deflection was measured by an LVDT, named LVDT_m, placed at the beam midspan (Figure 2). Two LVDTs, named LVDT_a and LVDT_b, measured possible vertical displacements at the beam supports (Figure 2). Since no significant displacements were measured by LVDT_a and LVDT_b, the beam vertical deflection was defined as the displacement measured by LVDT_m only.

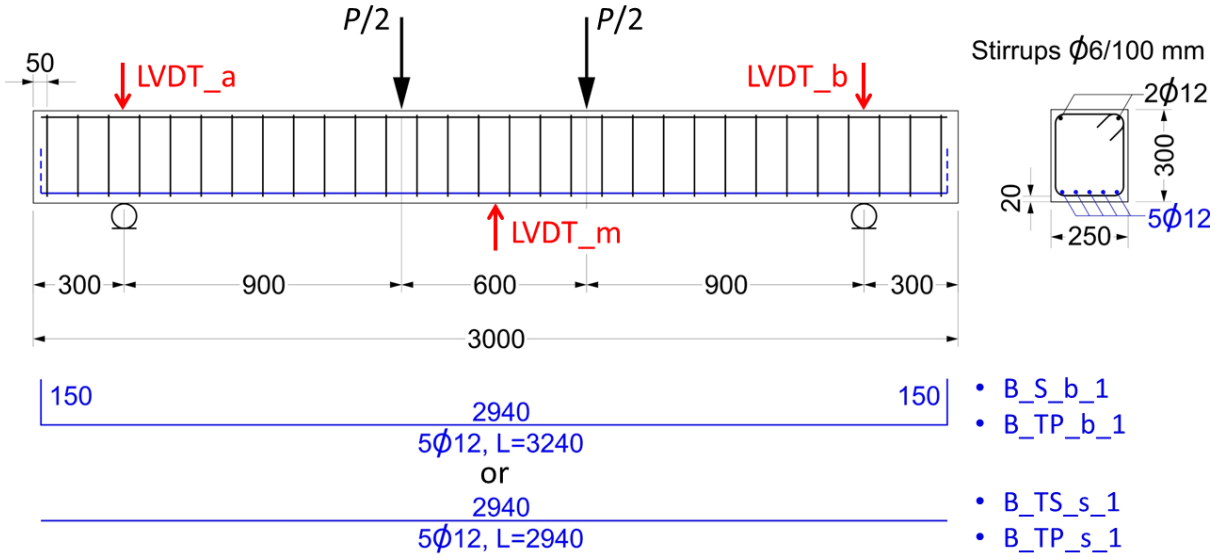

Figure 2: Geometry of beams tested (measures in mm)

Tests were carried out in displacement control by monotonically increasing the hydraulic jack stroke. Three load cycles were performed and the stroke rate ν varied depending on the reinforcement type (steel or GFRP). At the beginning of the test, the stroke was increased at a rate ν=0.0028 mm/s for all beams until the occurrence of concrete cracking. Then, the stroke was decreased until an applied load of approximately 1 kN and increased again until the applied load reached approximately 78 kN. This

load value was selected as representative of the service condition of the steel-reinforced concrete beam. After reaching such applied load, the stroke was decreased until an applied load of approximately 1 kN and increased again until failure of the beam. The stroke rate of the second cycle was ν=0.0170 mm/s and ν=0.0100 mm/s for the steel- and GFRP-reinforced beams, respectively, whereas that of the final cycle up to failure was ν=0.1360 mm/s and ν=0.0300 mm/s for the steel- and GFRP-reinforced beams, respectively.

Beams were named following the notation B_X_y_n, where B=beam, X=bar type (S=steel, TS=thermoset GFRP, TP=thermoplastic GFRP), y=bar shape (s=straight, b=bent), and n=specimen number.

EXPERIMENTAL RESULTS

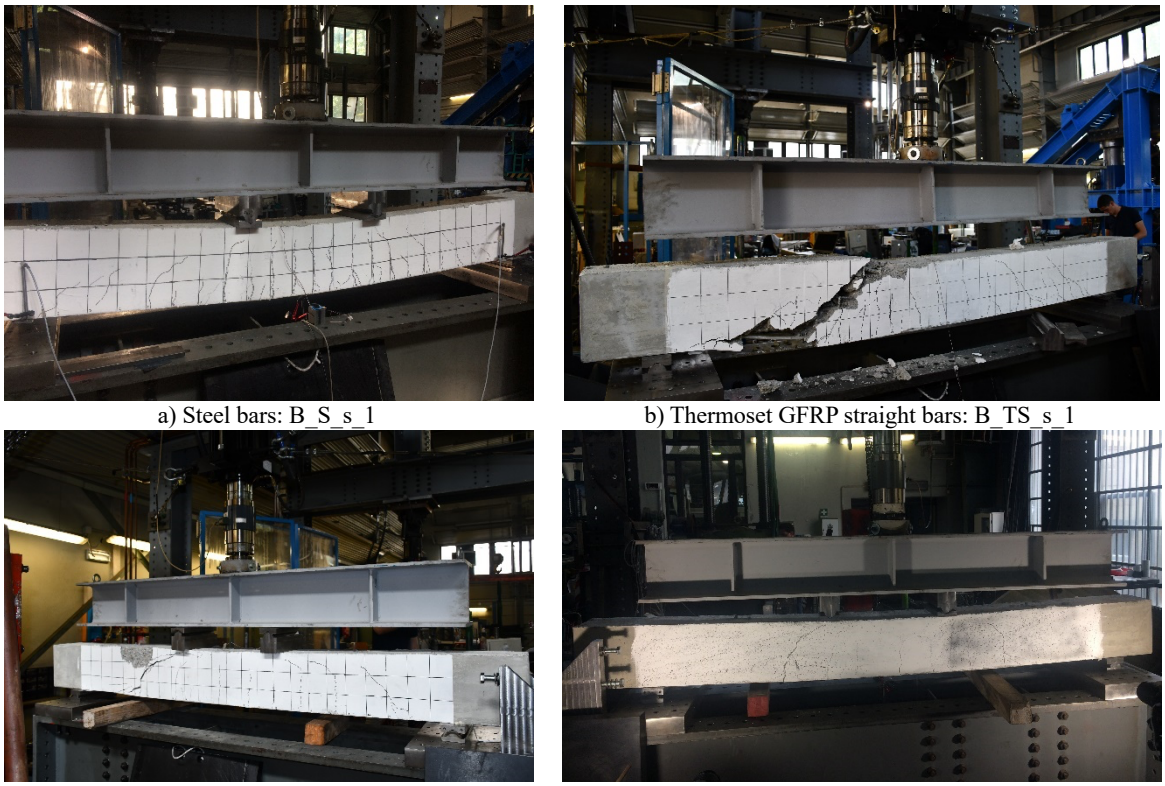

a) Steel bars: B_S_s_1

b) Thermoset GFRP straight bars: B_TS_s_1

c) Thermoplastic GFRP straight bars: B_TP_s_1

d) Thermoplastic GFRP bent bars: B_TP_b_1

Figure 3: Failure of beams reinforced with different types of bar

The beam reinforced with steel bars, i.e., specimen B_S_b_1, showed a ductile behavior with significant deflection and numerous vertical cracks concentrated in the beam central portion (Figure 3a). Its applied load P – vertical displacement δ curve, which is provided in Figure 4, clearly showed the occurrence of concrete cracking at an applied load P_{cr}=27.80 kN and the subsequent longitudinal steel yielding. Data obtained for vertical displacements between approximately 28 mm and 39 mm were omitted (a dashed line is reported in Figure 4) because they were affected by a set-up malfunctioning. For this reason, the beam was unloaded at δ equal to approximately 39 mm to allow for fixing this issue. Then, the specimen was tested up to δ~82 mm, when the test was interrupted due to the stroke limit of the hydraulic jack. The peak load obtained was P^*=190.17, which was associated with a vertical displacement δ^*=58.79 mm (Table 2).

The beam reinforced with thermoset GFRP straight bars, i.e., specimen B_TS_s_1, showed an initial behavior similar to that of beam B_S_s_1, with vertical cracks concentrated between the load application points (Figure 3b). Furthermore, concrete first cracking occurred at an applied load value (P_{cr}=29.20 kN, see Table 2) similar to that of beam B_S_s_1 (Figure 4). With increasing the machine

stroke after concrete first cracking, beam B_TS_s_1 showed a deflection higher than that observed for the same applied load in the steel-reinforced concrete beam, due to the elastic modulus lower for GFRP than for steel bars. Failure eventually occurred due the opening of a main shear crack (Figure 3b) at an applied load equal to P^*=164.93 kN (δ^*=36.94 mm, see Table 2).

Beams reinforced with straight (B_TP_s_1) and bent (B_TP_b_1) thermoplastic GFRP bars showed a behavior similar to that of beam B_TS_s_1, with the opening of vertical cracks in the central portion of the beam and eventual failure due to the opening of a main shear crack (Figure 3c and d). The load responses obtained resembled that of specimen B_TS_s_1, with some small differences: i) the applied load associated with concrete first cracking was lower (see Table 2) than that observed in beam B_TS_s_1 (and B_S_s_1) (Figure 4); and ii) the applied load associated with the shear failure was lower (see Table 2) than that of beam B_TS_s_1. These differences might be attributed to the different bond behavior of thermoset and thermoplastic GFRP bars. The results obtained suggested that, provided the same bonded length, the thermoplastic GFRP bar considered develops a lower tensile stress that the corresponding thermoset GFRP bar for the same value of interface slip.
The results obtained showed that bending the longitudinal thermoplastic GFRP bars ends did not affect the response obtained for the beams considered.

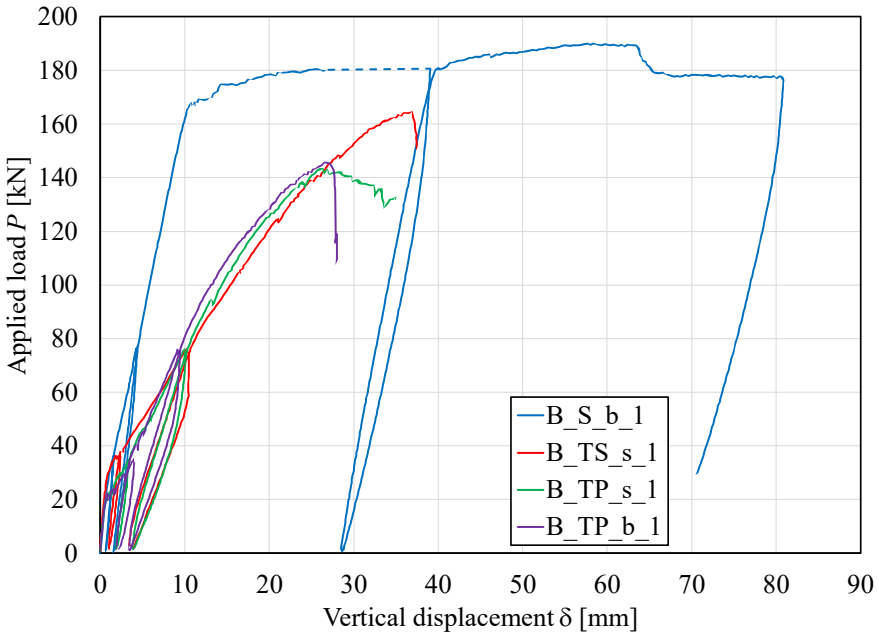

Figure 4: Applied load P – Vertical displacement δ of beams tested

Table 2: Cracking load P_{cr}, peak load P^*, and corresponding midspan vertical displacement δ^* of beams tested

Specimen	P_{cr} [kN]	P^* [kN]	δ^* [mm]
B_S_1	27.80	190.17	58.79
B_TS_1	29.20	164.93	36.94
B_TP_s_1	23.12	143.73	26.11
B_TP_b_1	21.56	146.11	31.10

DISCUSSION

In this work, the accuracy of existing formulations to predict the flexural and shear strength of concrete beams reinforced with steel or GFRP bars was assessed. The provisions of the Eurocode 2 (European Committee for Standardization, 2004), *fib* Bulletin 40 (Federation Internationale du Beton, 2007) and Italian guidelines CNR-DT 203 (National Research Council, 2007) were analyzed and their predictions compared with the corresponding experimental results. Even though *fib* Bulletin 40 (Federation Internationale du Beton, 2007) and Italian Guidelines CNR-DT 203 (National Research Council, 2007) are both currently being updated, they were considered in this paper for consistency

with the approach of the current Eurocode 2 (European Committee for Standardization, 2004). More recent formulations can be found in the literature (e.g., ACI 440.11 2022 (American Concrete Institute, 2015)).

The flexural strength of RC beams was computed under the hypothesis of plain sections remaining plane and of perfect bond between the concrete and reinforcement. The parabola-rectangle constitutive law was considered for concrete in compression (European Committee for Standardization, 2004), while the elastic-perfectly plastic law was assumed for steel bars. A linear elastic behavior up to failure was adopted for GFRP bars (Federation Internationale du Beton, 2007). Provided the material mechanical properties, the flexural capacity of the beam is computed applying two equilibrium equations to the beam cross-section (see Figure 5). Accordingly, the beam reinforced with steel bars attained failure due to concrete crushing, with the bottom longitudinal reinforcement yielded ($\varepsilon_s>\varepsilon_{yd}=f_{ym}/E_s$). The maximum (failure) bending moment M_{Rd} and $\xi=x/d$ obtained (x is the neutral axis depth and d=268 mm is the bottom reinforcement effective depth, see Figure 5) are reported in Table 3. To compare theoretical predictions and experimental results, $V_{Rd,M}$ and $P_{u,f}$ are also reported in Table 3, where $V_{Rd,M}=M_{Rd}/a$ (a=900 mm being the shear span) is the shear force along the shear span associated with the ultimate bending moment and $P_{u,M}=2V_{Rd,M}$ is the corresponding load applied by the testing machine. Partial and safety factors were not considered.

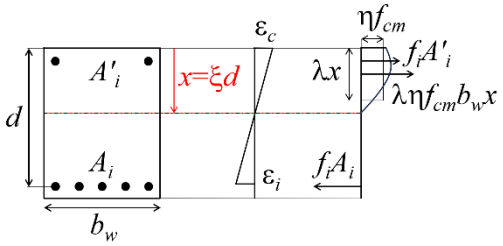

Figure 5: Strain and stress distribution of the RC beam cross-section

fib Bulletin 40 (Federation Internationale du Beton, 2007) introduces the balanced section reinforcement ratio, ρ_{fb}, which defines the amount of FRP reinforcement needed to a specific cross-section to simultaneously attain concrete crushing and FRP rupture (i.e., concrete and FRP simultaneously reach their maximum strain: $\varepsilon_c=\varepsilon_{cu}=0.0035$ and $\varepsilon_f=\varepsilon_{fu}=\bar{\sigma}_f^*/E_f$):

$$\rho_{fb}=\eta\lambda\frac{f_{cm}}{f_{fm}}\frac{E_f\varepsilon_{cu}}{E_f\varepsilon_{cu}+f_{fm}} \qquad \text{Eq. 1}$$

In Eq. 1, f_{cm}=44.8 MPa and $f_{fm}=\bar{\sigma}_f^*$. Thus, if $\rho_f>\rho_{fb}$ the cross-section fails due to concrete crushing while if $\rho_f<\rho_{fb}$ it fails due to FRP rupture. Accordingly, all GFRP bar-reinforced beams would attain bending failure due to concrete crushing (see first columns of Table 3). The maximum (failure) bending moment M_{Rd}, computed neglecting the contribution of the compressive reinforcement (Federation Internationale du Beton, 2007), is:

$$M_{Rd}=\eta f_{cm} b_w d^2(\lambda\xi)\left(1-\frac{\lambda\xi}{2}\right) \qquad \text{Eq. 2}$$

Results of this cross-sectional analysis are reported in Table 3.

Table 3: Results of cross-sectional analysis

Specimen	ρ_s [%]	ρ_f [%]	ρ_{fb} [%]	ξ [-]	M_{Rd} [kNm]	$V_{Rd,M}$ [kN]	$P_{u,M}$ [kN]
B_S_1	0.844			0.118	72.74	80.82	161.64
B_TS_1		0.884	0.477	0.179	107.33	119.26	238.51
B_TP_s_1		0.844	0.529	0.188	111.81	124.24	248.47
B_TP_b_1		0.844	0.529	0.188	111.81	124.24	248.47

The shear strength of RC beams was computed as

$$V_{Rd} = \min\left\{V_{Rd,i}, V_{Rd,max}\right\} \quad \text{Eq. 3}$$

where $V_{Rd,i}$ is the shear strength contribution of the internal transverse reinforcement (i.e., $V_{Rd,s}$) or the sum of internal transverse reinforcement and concrete resisting mechanisms contributions (i.e., $V_{Rd,ft}$) when steel or GFRP transverse reinforcement is employed, respectively, and $V_{Rd,max}$ is the shear strength provided by the concrete compressive strut, following the Mörsch truss analogy. According to Eurocode 2 (European Committee for Standardization, 2004), $V_{Rd,s}$ and $V_{Rd,max}$ were defined as:

$$V_{Rd,s} = \frac{A_{sw}}{s} f_{ywm} z \cot\theta \quad \text{Eq. 4}$$

$$V_{Rd,max} = \alpha_{cw} b_w z \nu_1 f_{cm} / (\cot\theta + \tan\theta) \quad \text{Eq. 5}$$

A_{sw}=56.5 mm^2 and s are the cross-sectional area and spacing of steel stirrups, f_{ywm}=505 MPa their yielding strength and z=0.9d=241.2 mm is the cross-section internal level arm. α_{cw} is a coefficient that takes into account the state of stress in the compression chord and is equal to 1 if no axial stress is present, ν_1=0.6 is a strength reduction factor for concrete cracked in shear and f_{cm} is the concrete mean compressive strength.

The shear strength contribution provided by GFRP transverse reinforcement was computed following the *fib* Bulletin 40 (Federation Internationale du Beton, 2007), which is based on the approach of the previous version of the Eurocode 2 (European Committee for Standardization, 1992) and employs the formulations of CNR-DT 203 (National Research Council, 2007). In this case, the beam shear strength is:

$$V_{Rd,ft} = V_{Rd,ct} + V_{Rd,f} \quad \text{Eq. 6}$$

$V_{Rd,ct}$ is the contribution of the concrete shear resisting mechanisms (i.e., resistance given by uncracked concrete in compression, aggregate interlock, and dowel action), specifically modified to account for the axial stiffness of the longitudinal reinforcement (Federation Internationale du Beton, 2007), while $V_{Rd,f}$ is the GFRP transverse reinforcement contribution.

$$V_{Rd,ct} = 1.3(E_f / E_s)^{1/2} \tau_{Rd} k(1.2 + 40\rho_l) b_w d \quad \text{Eq. 7}$$

$$V_{Rd,f} = \frac{A_{fw}}{s_f} f_{fr} d \quad \text{Eq. 8}$$

In Eq. 7, τ_{Rd}=0.25f_{ctk} =0.66 MPa is the concrete shear strength resistance, ρ_l=A_f/(db_w) is the longitudinal tension reinforcement ratio and k=(1.6-d)≥1. A_{fw} and s_f are the cross-sectional area and spacing of the FRP shear reinforcement and f_{fr} is the GFRP stirrup reduced strength. Since no specific experimental results were available, following the prescriptions of CNR-DT 203 (National Research Council, 2007), f_{fr} was taken as 50% of the corresponding (i.e., with the same diameter) GFRP straight bar tensile strength. Hence, $f_{fr} = 0.5\bar{\sigma}_f^*$ for thermoset (f_{fr}=610.0 MPa) and thermoplastic (f_{fr}=515.0 MPa) GFRP bars, respectively.

The shear strength contributions were computed with Eq. 3 - Eq. 5 for beam B_S_s_1 and with Eq. 3, and Eq. 5 - Eq. 8 for beams B_TS_s_1, B_TP_s_1, and B_TP_b_1. Results are reported in Table 4. Partial and safety factors were not considered and a fixed strut angle equal to 45° was assumed for all beams. In Table 4, $P_{u,S}$=2V_{Rd} is the load applied by the testing machine to attain beam shear failure.

Table 4: Shear capacity contributions according to the adopted guidelines

Specimen	$V_{Rd,max}$ [kN]	$V_{Rd,s}$ [kN]	$V_{Rd,f}$ [kN]	$V_{Rd,ct}$ [kN]	$V_{Rd,ft}$ [kN]	V_{Rd} [kN]	$P_{u,S}$ [kN]
B_S_1	665.43	68.88				68.88	137.76
B_TS_1	665.43		92.45	58.34	150.57	150.79	301.57
B_TP_s_1	665.43		78.05	61.30	139.35	139.35	278.69
B_TP_b_1	665.43		78.05	61.30	139.35	139.35	278.69

Comparisons between the theoretical shear and flexural capacities and the experimental loads at failure are reported in Table 5. According to the theoretical predictions, the steel-reinforced beam had a shear strength lower than the flexural strength (i.e., V_{Rd}<$V_{Rd,M}$). This result was not reflected in the failure mode obtained in the experimental test. However, it should be noted that a conservative value

of the concrete strut angle (45°) was assumed and that considering lower angles would entail for increase of the beam theoretical shear strength. Furthermore, the experimental peak load P^*=190.17 kN associated with bending failure was 17.65% higher than the theoretical prediction ($P_{u,M}$=161.64 kN), which can be explained by the steel longitudinal bar hardening, which was not accounted for in the analytical calculations. The theoretical predictions for GFRP-reinforced beams always provided higher shear than flexural strengths. However, all beams failed in shear. This could be attributed to the approximations made for the GFRP stirrup reduced strength.

Table 5: Comparison between theoretical predictions and experimental results

Specimen	M_{Rd} [kNm]	$V_{Rd,M}$ [kNm]	$P_{u,M}$ [kN]	V_{Rd} [kNm]	$P_{u,S}$ [kN]	P^* [kN]
B_S_1	73.11	81.20	162.50	68.88	137.76	190.17
B_TS_1	107.33	119.26	238.51	150.79	301.57	164.93
B_TP_s_1	111.81	124.24	248.47	139.35	278.69	143.73
B_TP_b_1	111.81	124.24	248.47	139.35	278.69	146.11

CONCLUSIONS

This paper provided and discussed the load response of four concrete beams reinforced with different longitudinal and transverse reinforcements and tested using a four-point bending configuration. One beam was reinforced with longitudinal and transversal steel reinforcement, whereas the remaining three beams were reinforced with the same cross-sectional area of GFRP bars. Namely, one beam was reinforced with thermoset GFRP bars whereas two beams with thermoplastic GFRP bars. For one of the beams reinforced with thermoplastic GFRP bars, the longitudinal bars were bent at the end.
The results obtained allowed for drawing the following main conclusions:

- The applied load associated with the concrete first cracking appeared to be affected by the presence and type of the bar. However, this observation needs to be confirmed by further investigations.
- Beams reinforced with thermoplastic GFRP bars provided a load response consistent with that of beams reinforced with thermoset GFRP bars. However, they provided a lower failure load, which was attributed to a different bar-concrete bond behavior.
- Bending of ends of longitudinal GFRP bars did not significantly affect the results.
- The theoretical predictions obtained by Eurocode 2, *fib* Bulletin 40, and CNR-DT 203 tended to overestimate the shear strength of the beams tested. Accurate measures of the GFRP stirrup reduced shear strength could improve the accuracy of these theoretical predictions.

ACKNOWLEDGEMENTS

The experimental tests described in this paper were conducted at the Laboratorio Prove Materiali of the Politecnico di Milano. Sireg Geotech srl is gratefully acknowledged for providing the composite bars.

CONFLICT OF INTEREST

The authors declare that they have no conflicts of interest associated with the work presented in this paper.

DATA AVAILABILITY

Data on which this paper is based is available from the authors upon reasonable request.

REFERENCES

Ahmed, E., Settecasi, F., & Benmokrane, B. (2014). Construction and Testing of GFRP Steel Hybrid-Reinforced Concrete Bridge-Deck Slabs of Sainte-Catherine Overpass Bridges. *Journal of Bridge Engineering*, *19*. https://doi.org/10.1061/(ASCE)BE.1943-5592.0000581

American Concrete Institute. (2015). *Guide for the Design and Construction of Structural Concrete Reinforced with Fiber-Reinforced Polymer Bars. ACI 440.1R-15*. https://www.concrete.org/store/productdetail.aspx?ItemID=440115&Format=PROTECTED_PDF&Language=English&Units=US_AND_METRIC

Benmokrane, B., Mousa, S., Mohamed, K., & Sayed-Ahmed, M. (2021). Physical, mechanical, and durability characteristics of newly developed thermoplastic GFRP bars for reinforcing concrete structures. *Construction and Building Materials*, *276*, 122200. https://doi.org/10.1016/j.conbuildmat.2020.122200

Carvelli, V., Pisani, M. A., & Poggi, C. (2010). Fatigue behaviour of concrete bridge deck slabs reinforced with GFRP bars. *Composites Part B: Engineering*, *41*(7), 560–567. https://doi.org/10.1016/j.compositesb.2010.06.006

D'Antino, T., Bertolli, V., Pisani, M. A., & Poggi, C. (2023). Tensile and interlaminar shear behavior of thermoset and thermoplastic GFRP bars exposed to alkaline environment. *Journal of Building Engineering*, *72*, 106581. https://doi.org/10.1016/j.jobe.2023.106581

D'Antino, T., & Pisani, M. A. (2023). Tensile and compressive behavior of thermoset and thermoplastic GFRP bars. *Construction and Building Materials*, *366*, 130104. https://doi.org/10.1016/j.conbuildmat.2022.130104

D'Antino, T., Pisani, M. A., & Poggi, C. (2018). Effect of the environment on the performance of GFRP reinforcing bars. *Composites Part B: Engineering*, *141*, 123–136. https://doi.org/10.1016/j.compositesb.2017.12.037

European Committee for Standardization. (1992). *Eurocode 2: Design of concrete structures—Part 1-1: General rules and rules for buildings*. CEN.

European Committee for Standardization. (2004). *Eurocode 2: Design of concrete structures—Part 1-1: General rules and rules for buildings*. CEN.

European Committee for Standardization. (2019). *Testing hardened concrete—Part 3: Compressive strength of test specimens. EN 12390-3:2019*. CEN.

Federation Internationale du Beton, C. J. (2007). *fib Bulletin 40. FRP reinforcement in RC structures* (fib. The International Federation for Structural Concrete, Ed.). fib. The International Federation for Structural Concrete. https://doi.org/10.35789/fib.BULL.0040

ISO 10406-1:2015. (2015). *Fibre-reinforced polymer (FRP) reinforcement of concrete—Test methods*. ISO. https://www.iso.org/cms/render/live/en/sites/isoorg/contents/data/standard/06/36/63657.html

Januš, O., Girgle, F., Rozsypalová, I., Kostiha, V., Bodnárová, L., Štěpánek, P., & Prokeš, J. (2019). The fatigue behaviour of GFRP bars—Experimental study. *Acta Polytechnica CTU Proceedings*, *22*, 38–47. https://doi.org/10.14311/APP.2019.22.0038

Kocaoz, S., Samaranayake, V. A., & Nanni, A. (2005). Tensile characterization of glass FRP bars. *Composites Part B: Engineering*, *36*(2), 127–134. https://doi.org/10.1016/j.compositesb.2004.05.004

National Research Council. (2007). *Guide for the Design and Construction of Concrete Structures Reinforced with Fiber-Reinforced Polymer Bars. CNR-DT 203/2006*. CNR.

Solyom, S., & Balázs, G. L. (2020). Bond of FRP bars with different surface characteristics. *Construction and Building Materials*, *264*, 119839. https://doi.org/10.1016/j.conbuildmat.2020.119839

Zhao, X., Minhajur Rahman, M., D'Antino, T., Focacci, F., & Carloni, C. (2022). Effect of bonded length on the load response and failure mode of pull-out tests of GFRP bars embedded in concrete. *Construction and Building Materials*, *347*, 128425. https://doi.org/10.1016/j.conbuildmat.2022.128425

Zoller, A., Escalé, P., & Gérard, P. (2019). Pultrusion of Bendable Continuous Fibers Reinforced Composites With Reactive Acrylic Thermoplastic ELIUM® Resin. *Frontiers in Materials*, *6*. https://www.frontiersin.org/articles/10.3389/fmats.2019.00290